SSRG International Journal of Electrical and Electronics Engineering
ISSN: 2348-8379/ https://doi.org/10.14445/23488379/IJEEE-V13I2P108

Volume 13 Issue 2, 110-117, February 2026

Original Article

Design and Implementation of Full-Bridge Resonant Inverter with PLL Control for Induction Welding Applications

B. Sriboonrueng[1], J. Jittakort[1*], A. Aurasopon[2], N. Saengngam[1]

[1]*Department of Electrical Engineering, Faculty of Technical Education, Pathum Thani, Thailand.*
[2]*Faculty of Engineering, Mahasarakham University, Mahasarakham, Thailand.*

[*]*Corresponding Author : jirapong_j@rmutt.ac.th*

Received: 16 November 2025 Revised: 19 December 2025 Accepted: 17 January 2026 Published: 17 February 2026

Abstract - *This paper presents the design and implementation of a Full-Bridge Resonant (FBR) inverter employing Zero-Voltage Switching (ZVS) for induction welding applications. The proposed system aims to improve efficiency, reduce switching losses, and achieve a compact and lightweight welding power supply. The inverter is designed to operate at a high switching frequency of 35 kHz with an input voltage of 400 VDC and a maximum output current of 120 A, delivering a rated output power of 9.6 kW. A Phase-Locked Loop (PLL) control system implemented on a TMS320F28335 DSP is used to synchronize the inverter's switching frequency with the resonant current, ensuring stable ZVS operation under varying load conditions. Simulation and experimental results verify that the inverter achieves smooth and stable arc welding performance. The measured output voltage and current are approximately 60–80 V and 110–120 A, respectively, producing a uniform weld bead with minimal spatter and excellent penetration. The experimental prototype demonstrates that the proposed FBR inverter provides high efficiency, stable operation, and reduced thermal stress on power switches. With its compact design and high power density, the inverter is suitable for modern welding systems. It can also be applied to other high-frequency industrial processes such as induction heating and metal melting applications.*

Keywords - *Full-Bridge Resonant Inverter, Zero-voltage Switching, Phase-Locked Loop, DSP Control, Induction Welding.*

1. Introduction

The arc welding application is essential in metal manufacturing, building, and maintenance**.** The stability and accuracy of the welding arc are essential elements that directly influence weld quality. However, the Conventional Welding Power supplies, mostly reliant on linear technology or 50 Hz transformer systems, continue to exhibit numerous drawbacks, such as substantial dimensions, considerable weight, and diminished energy efficiency. Industry requirements are shifting towards lightweight, portable equipment**.** The growing requirement for an advanced power supply that can offer improved arc stability and optimize overall welding performance. The high switching frequency technology of the power electronic part of the resonant inverter has considerably reduced these constraints. The whole bridge resonant inverter implemented under the ZVS can reduce and minimize the switching losses. Operating at high frequency helps reduce the size of passive components, such as transformers and capacitors, resulting in a more compact and lightweight welding power supply. Furthermore, the ZVS operation supports the power switching devices, such as IGBTs or MOSFETs, to operate with less energy loss.

The full- bridge resonant inverter can reduce Electromagnetic Interference (EMI) and switching losses by maintaining ZVS operation across the power switch. This technique enables high- frequency switching, resulting in faster power supply response and more accurate control of the welding current. Moreover, resonant operation enables the inverter to provide a stable power output, important for maintaining consistent arc characteristics during demanding welding techniques such as Tungsten Inert Gas (TIG) Welding, Shielded Metal Arc Welding (SMAW), and Metal Inert Gas (MIG) Welding.

The ZVS resonant inverter using the Synchronous Rectification (SR) can reduce conduction losses during the rectification phase. The SR method replaces conventional traditional diodes with MOSFETs, therefore minimizing voltage drop and thermal losses, particularly under elevated output current situations. Considering the ZVS full- bridge resonant inverter's apparent benefits in efficiency, compactness, and operational stability, challenges remain, especially with arc dynamics, disturbance management, and real- time control of the welding process. The Field-

Programmable Gate Arrays (FPGAs) for accurate real-time regulation are to improve the efficacy of the welding power supply.

However, the resonant inverter under the operation of the ZVS condition, with the advantage of high efficiency for the soft switching and compact size, has been proposed in the induction heating application. More research aims to consider the steady-state response with light to medium power. In part of the resonant frequency tracing, the load parameter variation for the transient response is neglected. Additionally, an analog control for the pulse width modulation for the arc welding application is unresponsive to the real-time transient response of the dynamic load for the high-power application.

In this paper, an improved full-bridge resonant inverter with a tracking resonant frequency is proposed. The aim is to control the output power of induction welding for high-temperature applications, where both the load parameters and the resonant frequency vary significantly during system operation. Moreover, the improved efficiency of the full-bridge resonant inverter is operated under ZVS conditions. The operating frequency is controlled using a phase-locked loop to track the resonant frequency that is generated by the DSP of the TMS320F28335 from Texas Instruments. The arrangement of this paper is organized as follows. The literature review, background, highlighting, and significance are presented in Section 2. The control strategy, circuit configuration, and operating principle of the full-bridge resonant inverter for electric welding applications are described in Section 3. Section 4 proposes the design of the key parameters of the full-bridge resonant inverter. Section 6 explains the implementation of the inverter system controlled by a DSP. Simulation and experimental results are discussed in Section 6. Section 7 concludes this paper.

2. Literature Review

The various types of arc welding applications, such as MAG, TIG, and SMAW, are essential in the industry that requires a precise and stable power supply in the design of the welding power sources. Many teachings demand improving the efficiency of the welding application, such as the resonant inverter, synchronous rectification, and digital control methods. Power Electronic Technology in the part of the resonant converters is becoming widely used in the arc welding application because of reduced size and improved efficiency. In reference [1], the resonant inverter was proposed to minimize switching losses. This work is focused on reducing the size and weight of the transformer in the arc welding machine. This paper is combined with interleaving and synchronous rectification, further improving the performance by reducing output current fluctuations and increasing efficiency, especially during standby operations. The FPGA technology presents an improvement in the regulation of the arc welding power supply. Reference [2] underlines the use of FPGA-based digital controllers to improve the performance of resonant inverters in real-time**.** The systems offer regulation of the welding current, which meets the requirements of numerous welding processes, such as MIG, TIG, and SMAW.

The arc welding of SMAW, which includes nonlinear processes, arc variations, and short circuits, has already been presented in reference [3], which may lead to welding defects such as metal spatter and uncertain arc instability. As referenced in [4], the presented driver circuit simplifies the operation of the IGBT power switches in the inverter for the welding application. The pulse width modulation using the digital microcontroller to drive the inverter has low cost and stability. In Previous Study, other applications, such as the ultrasonic cleaner, used the full-bridge resonant inverter, which minimized power loss, to maintain ZVS operation throughout the load variation. Moreover, this method was used to track resonance frequencies using the PLL scheme.

The reference [5] presents a high switching frequency to drive the resonant inverter for the Wireless Power Transfer (WPT) application. In reference [6], the resonant inverter for WPT offers the advantage of ZVS operation to minimize power loss; however, it has the limitation of a narrow control range during load variations due to the inconsistent DC input voltage of the inverter. Additionally, reference [7] proposed the resonant inverter for the Photovoltaic Systems that achieves the ZVS operation under optimal conditions. The single-phase ZVS full-bridge inverter that uses active power decoupling control has been proposed in reference [8], which alleviates double-frequency ripple on the DC-link capacitor. This method improves efficiency and reduces the size of the electrolytic capacitors.

In reference [9], the high-power application of the hybrid clamped three-level full-bridge resonant inverter that employs the ZVS operation to minimize the thermal distribution has been proposed. This method ensures that the high-power system maintains a wide voltage range while the load parameters vary. The hybrid microgrid system designed for renewable energy applications, which features an AC voltage input for the converter, is presented previous study; this system utilizes a bidirectional converter to manage and stabilize power flows. That system improves the efficiency of the AC-to-DC converter. The resonant frequency tracking load variation of the Piezoelectric Transformer based on the PLL technique with the resonant inverter operated under ZVS condition has been proposed in the reference [10]. Moreover, this method presents the technique to accurately control the dead time with the PLL algorithm and can reduce the EMI effect of the inverter.

The reference [11] presents the improved PLL scheme that uses the Newton-Raphson-based PLL with a PI controller for sensorless motor drive systems, stating that this method combines with an extended state observer. That method can

reduce the steady- state errors of the proposed system. Reference [12] presents the four-leg Z-source inverter with common-mode voltage based on the DSP of TMS320F28335 for the solar system, which can reduce leakage current and respond quickly to control, improving efficiency. In the reference [13], the smart 3-phase 4-leg voltage-source inverter is presented to improve the power quality in the four wires of the distribution systems based on the DSP of TMS320F28335 with real-time control. This system can reduce the component of neutral current and adjust the optimized load. Moreover, the controller of this system can control the fast interrupt current of the nonlinear load. The previous study presents the Piezoelectric Ceramic Transducer designed to drive the ultrasonic cleaner application, which is based on the class E voltage source resonant inverter and includes a CLC filter to reduce acoustic noise and EMI. That research uses the PLL to track the resonant frequency of the variation of the parameter of the Piezoelectric Ceramic Transducer while the liquid solvent of the ultrasonic is varying. The gate drive control for the inverter uses the DSP of TMS320F28335.

3. Proposed system

3.1. Full Bridge Resonant Inverter System Configuration

Figure 1 shows the proposed system configuration that consists of the full-bridge resonant inverter, the series resonant capacitor, C_r, the matching transformer, T_{r1}, the rectifier, and the arc welding load. The full-bridge resonant inverter consists of four power switch devices, such as the IGBTs. The output voltage of the full-bridge resonant inverter at points *a* and *b*, identified as $v_{ab}(t)$ and the current through the resonant load, indicated as $i_{inv}(t)$ are detected for the input signals of the control unit. Figure 2 shows the necessary waveforms of the full-bridge resonant inverter for the arc welding load during steady- state operation under ZVS conditions, where the switch frequency, f_s exceeds the resonant frequency. The waveforms of the four gate signals for switches $Q_1 - Q_4$, the voltage across the power switch Q_1 at pins *C* and *E*, denoted as $v_{CE\_Q1}(t)$, the current through pin *C* of the power switch Q_1, represented as $i_{C\_Q1}(t)$, $v_{ab}(t)$, $i_{inv}(t)$, and the fundamental voltage of the waveform of $v_{ab}(t)$ and $v_{ab1}(t)$.

3.2. Modes of Operation

The operational modes of the full-bridge resonant inverter at steady state, as depicted in Figure 2, consist of four different modes of operation. Each mode is shown in Figure 3.

In Mode 1, as depicted in Figure 3(a), during the time interval from t_1 to t_2, diodes D_1 and D_4 are activated, allowing the current $i_{inv}(t)$ to pass via a diode D_4, transformer T_{r1}, and a diode D_1, while the output current I_o The rectifier is a positive current flowing through the arc welding load.1

In Mode 2, shown in Figure 3(b), during the interval from t_2 to t_3, switches Q_1 and Q_4 are switched on, allowing the current $i_{inv}(t)$ to flow through switch Q_1, transformer T_{r1}, and switch Q_4, while the output current I_o The rectifier provides a positive current flowing through the arc welding load. This mode enables the full-bridge resonant inverter to achieve ZVS operation. In Mode 3, represented in Figure 3(c), during the interval t_3 to t_4, diodes D_2 and D_3 are activated, allowing the current $i_{inv}(t)$ to flow through a diode D_2, transformer T_{r1}, and a diode D_3, while the positive output current I_o passes through the arc welding load. In this mode, the voltage $v_{ab}(t)$ is negative.

In Mode 4, as shown in Figure 3(d), from t_4 to t_5, switches Q_2 and Q_3 are activated, allowing the negative current $i_{inv}(t)$to flow through switch Q_2, transformer T_{r1}, and switch Q_3, while the output current I_o The rectifier delivers a positive current to the arc welding load. In this mode, the voltage $v_{ab}(t)$ is negative Figure 3.

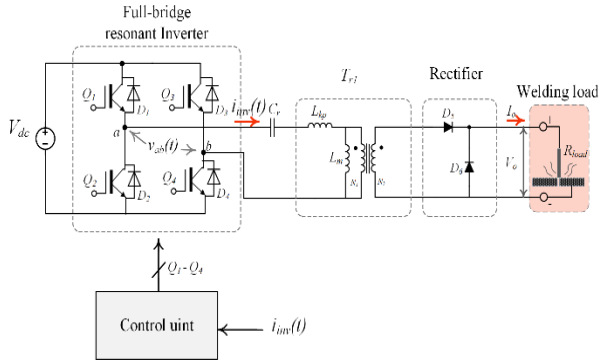

Fig. 1 Full-bridge resonant inverter for arc welding load

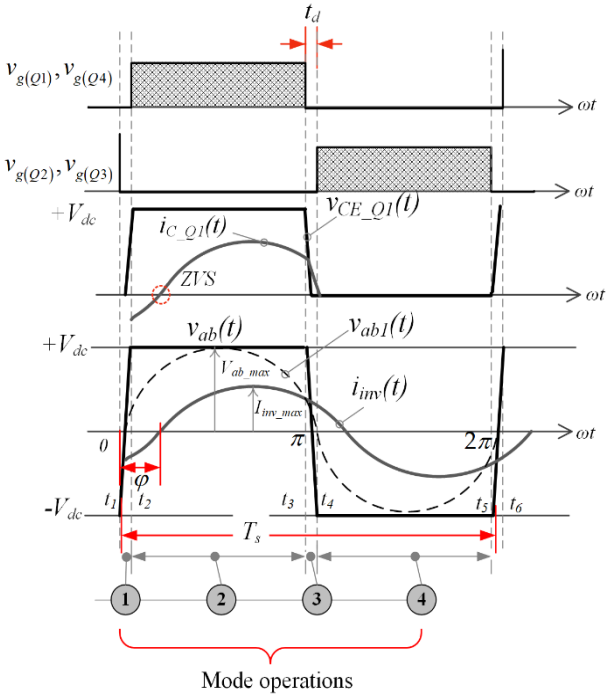

Fig. 2 Key waveforms of the full-bridge resonant inverter

The voltage gains of the resonant tank, $M_{again}(s)$, represent the transfer function that correlates the output voltage to the input voltage, as indicated in Equation (1).

$$M_{gain}(s) = \left|\frac{V_{oac}(s)}{V_{ab1}(s)}\right| = \frac{(f_s/f_r)^2(k-1)}{\sqrt{(k(f_s/f_r)^2-1)^2+(f_s/f_r)^2((f_s/f_r)^2-1)^2(k-1)^2Q_L^2}} \quad (1)$$

Where the ratio of total primary inductance to resonant inductance $k = (L_r + L_m)/L_r$ is and the resonant frequency, f_r, is $1/(2\pi\sqrt{L_rC_r})$.

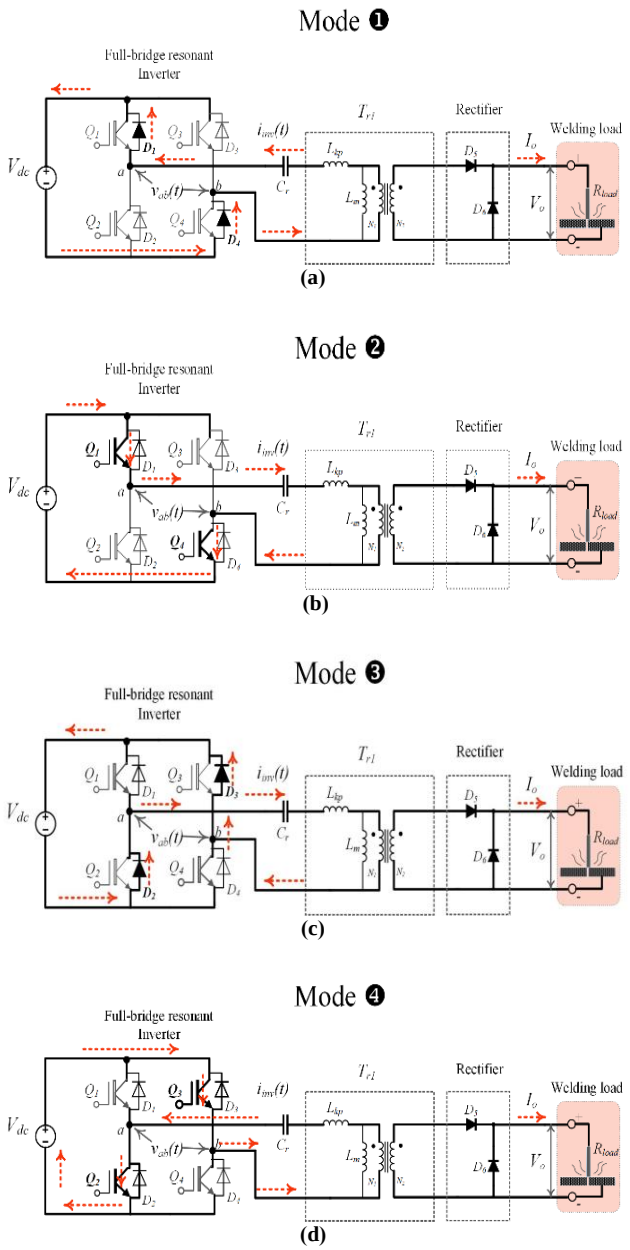

Fig. 3 Mode operations of the full-bridge resonant inverter

The load quality is

$$Q_L = \frac{\sqrt{L_r/C_r}}{R_{ac}} \quad (2)$$

The reflected load resistance is

$$R_{ac} = \frac{8n^2R_{load}}{\pi^2} \quad (3)$$

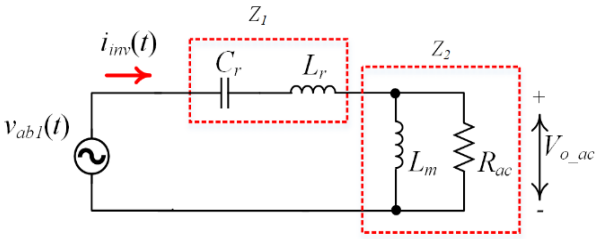

Fig. 4 Equivalent circuit of full-bridge resonant inverter

The total impedance of the equivalent circuit in Figure 4 is:

$$Z_{total} = \underbrace{-\frac{j}{\omega C_r} + j\omega L_r}_{Z_1} + \underbrace{\frac{R_{ac}j\omega L_m}{\omega C_r + j\omega L_m}}_{Z_2} \quad (4)$$

Thus, the magnitude or fundamental part of Z_{total} is:

$$|Z_{total}| = \sqrt{\left(-\frac{j}{\omega C_r} + j\omega L_r + \frac{R_{ac}j\omega L_m}{R_{ac}+j\omega L_m}\right)^2} \quad (5)$$

In order to represent the periodic function of voltage $v_{ab}(t)$ of the full-bridge resonant inverter, which can be seen in Figure 2, the following Fourier series can be expressed:

$$v_{ab}(t) = \frac{4V_{dc}}{\pi}\sum_{n=1,3,5,\ldots}^{\infty}\frac{1}{n}sin(2\pi n f_s t) \quad (6)$$

Where the fundamental amplitude of the voltage $v_{ab}(t)$ is $V_{ab1} = 4V_{dc}/\pi$. The average power of a full- bridge resonant inverter can be determined by

$$P_{inv} = \frac{V_{ab1}^2}{|Z_{total}|} \quad (7)$$

4. System Design

The specifications for the design of the full- bridge resonant inverter for the arc welding equipment are as follows. The output current I_o at full load is specified as 120 A, while the no- load output voltage V_o is 80 V. The designated parameters for the design of the full-bridge resonant inverter are provided in Table 1. The turn ratio of the transformer is:

$$a = \frac{V_1}{V_2} = \frac{400}{80} = 5.0$$

Where the transformer T_{r1} Primary and secondary voltages are V_1 and V_2, respectively. The load resistor is:

$$R_{ac} = \frac{V_o^2}{P_o} = \frac{(80)^2}{9{,}600} = 0.667\ \Omega$$

Table 1. The Specified Parameters of the Full-Bridge Resonant Inverter

Parameters	values
Input voltage *(V_{dc})*	400 V
Switching frequency *(f_s)*	35 kHz
Resonant capacitor *(C_r)*	30 nF
Maximum load current I_o	120 A
No-load output voltage V_o	80 V
Output power P_o	$P_o = I_o V_o$ =9.6 kW

The reflected load resistance is:

$$R_{ac} = \frac{8n^2 R_{load}}{\pi^2} = \frac{8\times 5^2 \times 0.667}{\pi^2} = 13.5\ \Omega$$

The load quality is determined by,

$$Q_L = \frac{\sqrt{L_r/C_r}}{R_{ac}}.$$

To guarantee the ZVS condition for the LLC converter, set Q_L to 0.5. Therefore, the inductance L_r is calculated as follows:

$$L_r = C_r(Q_L R_{ac})^2 = 1.0\ mH$$

The inductance factor k is L_m/L_r where k is set to 5. Therefore, the magnetizing inductance L_m is equal to 0.5 mH. The design of a high-frequency transformer for an electrical welding load can be demonstrated using the following method. Transformer design using EE core assumptions: the core area is $A_e = 400\ mm^2 = 4 \times 10^{-4}\ m^2$

$$N_1 = \frac{V_p}{4.44 f_s B_m A_e} \approx 32\ turns$$

where the secondary turns is,

$$N_2 = \frac{N_1}{5} \approx 7\ turns$$

The design of power switch devices for a full-bridge resonant inverter is shown as follows. The IGBT voltage rating is:

$$V_{CE\_IGBT} > 2V_{dc} > 800\ V$$

The root mean square (*rms*) current on the primary side of the transformer T_{r1} is

$$I_{inv\_rms} = \frac{I_{sec\_rms}}{5} = \frac{120\ A}{5} = 24\ A$$

where I_{sec_rms} is the *rms* current on the secondary side of the transformer T_{r1}.

The collector current of the power switch IGBT is

$$I_{C\_IGBT} = 1.5 I_{inv\_rms} = 36\ A$$

The output current for each fast recovery diode during conduction is:

$$I_{avg\_diode} = 1.5\left(\frac{I_o}{2}\right) = 67.50\ A$$

where the reverse voltage is 100 V.

5. Implementation

Figure 5 illustrates the welding system of the full-bridge resonant inverter, which is designed for welding loads and incorporates a specific control method. The whole bridge inverter is composed of switching devices. $Q_1 - Q_4$ and diodes $D_1 - D_4$. The function of the inverter is to convert the voltage. V_{dc} to the output voltage waveform between points a and b ($v_{ab}(t)$). The resonant tank consists of the resonant capacitor. C_r and the leakage or magnetizing inductance of the high-frequency transformer T_{r1}.

This proposed system enables the ZVS operation, reducing switching losses and improving efficiency. The transformer T_{r1}, with the primary and secondary windings L_p and L_m, is to adjust the voltage and current levels before the signal passes through the rectifier of D_5 and D_6. The zero-crossing detector circuit raises the signal level of the sinusoidal waveform of the current. $i_{inv}(t)$, that is, to obtain a voltage level of 0 to 3.3 volts.

The signal generator for pulse width modulation of the resonant inverter uses the DSP of TMS320F28335. The input signal at the ADC port of the DSP is the signal of the current. $\boldsymbol{i_{inv}(t)}$ from the zero-crossing detector circuit that passes through the block diagram of the low-pass filter of the PLL control. Then, the actual current of the current $i_{inv}(t)$ is compared with the output current command. The error signal of the comparator is compensated by a current controller as a PI controller.

Then, the signal is the input command of the phase angle between the output voltage of the $v_{ab}(t)$ and the current $i_{inv}(t)$, which is adjusted and compensated by the Voltage-Controlled Oscillator (VCO).

The dead time for the gate drive circuit is set to 1.5 µs. The gate drive circuit of the inverter uses four opto-isolators, TLP250 from Toshiba. The experimental setup of the full-bridge resonant inverter for the arc welding is shown in Figure 6.

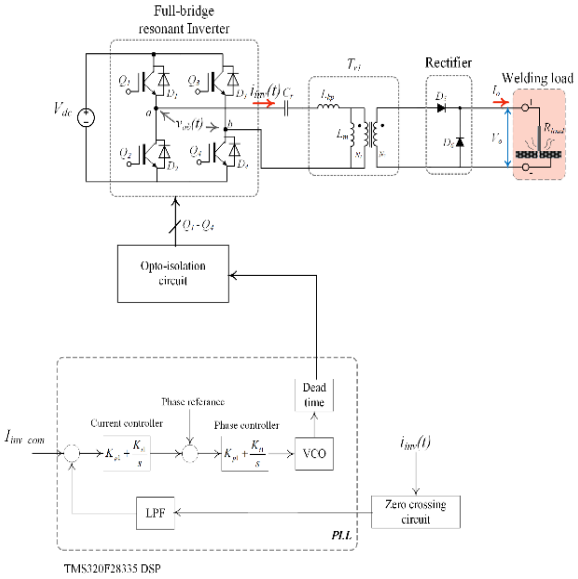

Fig. 5 Full-bridge resonant inverter operation system

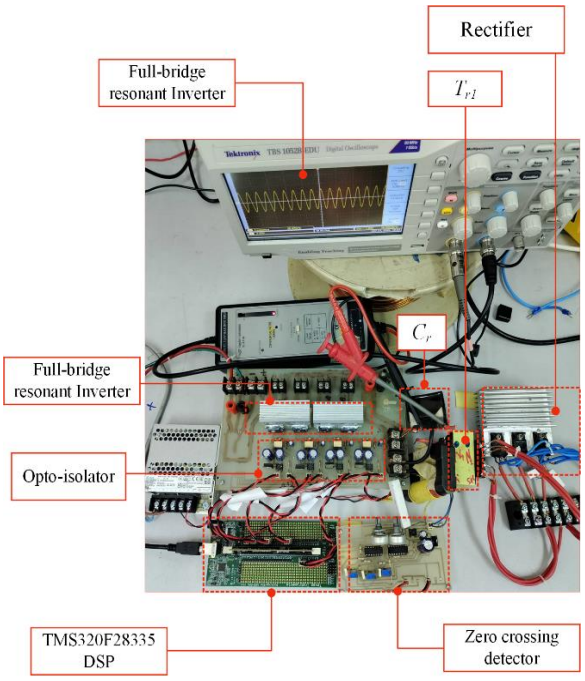

Fig. 6 Implement System

6. Results

6.1. Simulation Results

The simulation results of the full-bridge resonant inverter for the arc welding load at 80% of full load are shown in Figures 7 and 8. Figure 7 shows the simulation results for the current I_{o_com}, voltage V_o, and current I_o, respectively.

The current I_{o_com} is 120 A at a voltage V_o of 65 V, with the current I_o also at 120 A. The results of the simulation indicate that the control system of the full-bridge resonant inverter with PLL.

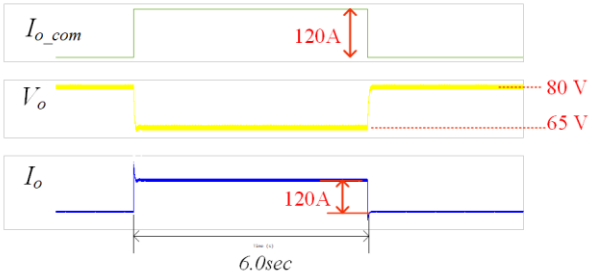

Fig. 7 Simulation results of full-bridge resonant inverter for arc welding load

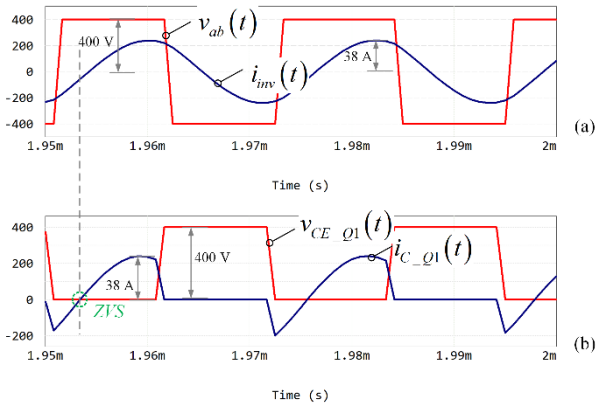

Fig. 8 Simulation results (a) The voltage $v_{ab}(t)$ and The current $i_{inv}(t)$, and (b) The voltage $v_{CE\_Q1}(t)$ and the current $i_{C\_Q1}(t)$.

The control can precisely follow the reference current. The simulation results for the arc welding load applied using the full-bridge resonant inverter are displayed in Figure 8. The simulation results for the peak voltage $v_{ab}(t)$ and peak current $i_{inv}(t)$ are 400 V and 38 A, respectively, as seen in Figure 8(a). The simulation results of the full-bridge resonant circuit record the ZVS operation of the peak voltage $v_{CE\_Q1}(t)$ and peak current of $i_{C\_Q1}(t)$ are 400 V and 38 A, respectively, as shown in Figure 8(b).

6.2. Experimental Results

The experimental results of the inverter for arc welding load are measured by a digital oscilloscope (Tektronix, TBS 1052B-EDU). Figure 9 shows the experimental results of the full-bridge resonant inverter for an arc welding load, with a current I_o of 110 A and a voltage V_o of 65 V, respectively. The power P_o The arc welding application is 6.6 kW. Figure 10 shows the experimental results of the voltage. $v_{ab}(t)$and current $i_{inv}(t)$ for the full-bridge resonant inverter arc welding load at a switching frequency of 36.5 kHz. Figure 10(a) shows the voltage $v_{ab}(t)$ and current $i_{inv}(t)$ of the full-bridge resonant inverter, with a time per division of 1 second. Figure 10(b) shows the voltage $v_{ab}(t)$ and current $i_{inv}(t)$ of the full-bridge resonant inverter, with a time per division of 5 µs, where the peak voltage $v_{ab}(t)$ is 310 V and the peak current $i_{inv}(t)$ is 34 A. The experimental results for the peak voltages $v_{ab}(t)$ of 310 V and $v_1(t)$ of 438 V are displayed in Figure

11. Figure 12 shows the ZVS operation of the full-bridge resonant inverter, with the experimental results of the peak voltage $v_{ab}(t)$ of 310 V and current $i_{C\_Q1}(t)$ of 34 A. Figure 13 shows the welding results of the mild steel with a thickness of 3 mm and a weld length of 7 cm. According to the welding results, the surface of the weld has a continuous ripple pattern and is smooth. During the welding process, the inverter is able to maintain the ZVS condition.

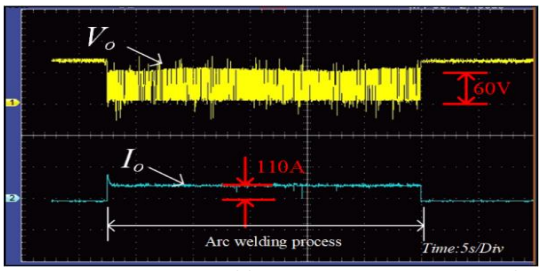

Fig. 9 Experimental results of full-bridge resonant inverter for arc welding load

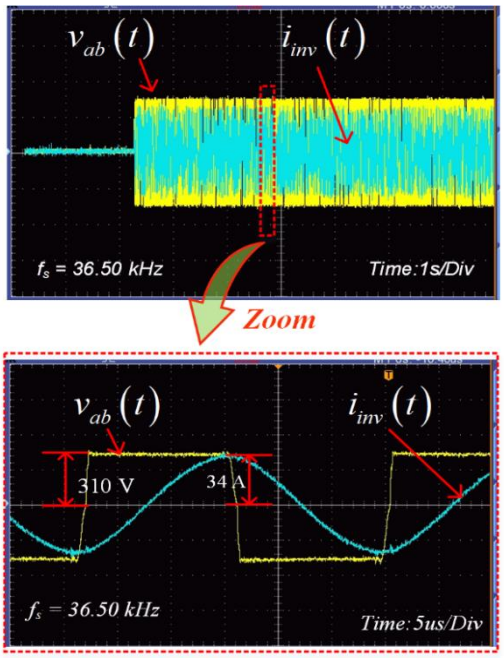

Fig. 10 Experimental results (a) The voltage $v_{ab}(t)$ and the current $i_{inv}(t)$, and (b) The voltage $v_{CE\_Q1}(t)$ and the current $i_{C\_Q1}(t)$.

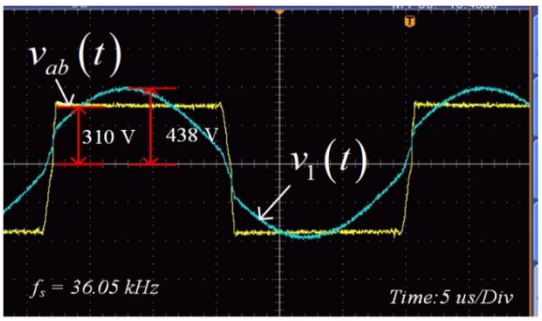

Fig. 11 Experimental results of voltage $v_{ab}(t)$ and $v_1(t)$.

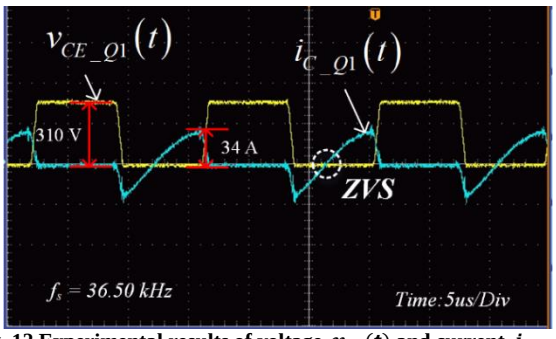

Fig. 12 Experimental results of voltage $v_{ab}(t)$ and current $i_{C\_Q1}(t)$

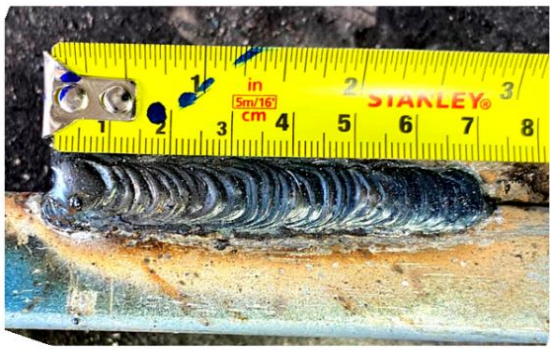

Fig. 13 Welding line for mild steel

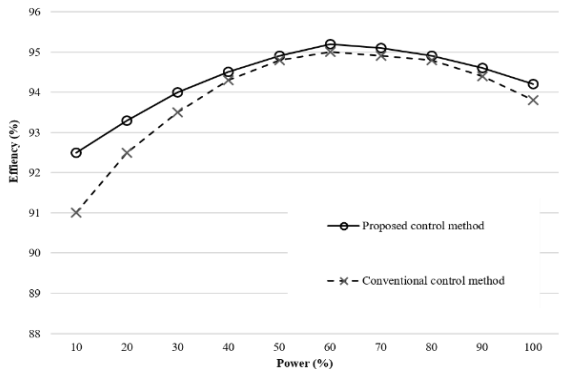

Fig. 14 The proposed control method with the conventional control methods used in arc welding applications

Figure 14 shows the experimental results of the inverters using the proposed control and the conventional control. For maximum output power, the output power between 50% and 100% indicates the proposed control has slightly more efficiency than the conventional control method, but for low output power in the range of 10% to 40%, the proposed control has the same efficiency as the conventional control method.

7. Conclusion

The design and implementation of a full-bridge resonant inverter for the induction welding application clearly demonstrate the effectiveness of ZVS operation at high frequencies. The proposed system uses the PLL control method provided by the TMS320F28335 DSP processor to control the full-bridge resonant inverter. This technique

achieves soft switching, where the inverter maintains ZVS operation though the welding load varies. The result is smooth and uniform, and the welding process can be carried out rapidly. The simulation and experimental results of the full-bridge resonant inverter have the performance and stability during the welding process that can confirm the proposed scheme. Therefore, the proposed system, which includes the presented circuit configuration and resonant frequency tracking control method, can be applied to other applications requiring output regulation under varying load conditions.

References

[1] Alejandro Navarro-Crespin, Rosario Casanueva, and Francisco J. Azcondo, "Performance Improvements in an Arc-Welding Power Supply based on Resonant Inverters," *IEEE Transactions on Industry Applications*, vol. 48, no. 3, pp. 888-894, 2012. [CrossRef] [Google Scholar] [Publisher Link]

[2] Alejandro Navarro-Crespin et al., "Digital Control for an Arc Welding Machine based on Resonant Converters and Synchronous Rectification," *IEEE Transactions on Industrial Informatics*, vol. 9, no. 2, pp. 839-847, 2013. [CrossRef] [Google Scholar] [Publisher Link]

[3] Arun Kumar Paul, "Robust Product Design using SOSM for Control of Shielded Metal Arc-Welding (SMAW) Process," *IEEE Transactions on Industrial Electronics*, vol. 63, no. 6, pp. 3717-3724, 2016. [CrossRef] [Google Scholar] [Publisher Link]

[4] Jayasheela Deepa Jabavathi, and Habeebullah Sait, "Design of a Single Chip PWM Driver Circuit for Inverter Welding Power Source," *IEEE Transactions on Circuits and Systems II: Express Briefs*, vol. 67, no. 4, pp. 720-724, 2020. [CrossRef] [Google Scholar] [Publisher Link]

[5] Yenan Chen, Minjie Chen, and Dehong Xu, "A 3-kW Two-Stage Transformerless PV Inverter with Resonant DC Link and ZVS-PWM Operation," *IEEE Transactions on Industry Applications*, vol. 57, no. 2, pp. 1495-1506, 2021. [CrossRef] [Google Scholar] [Publisher Link]

[6] Hamed Tebianian et al., "A 13.56-MHz Full-Bridge Class-D ZVS Inverter with Dynamic Dead-Time Control for Wireless Power Transfer Systems," *IEEE Transactions on Industrial Electronics*, vol. 67, no. 2, pp. 1487-1497, 2020. [CrossRef] [Google Scholar] [Publisher Link]

[7] Anh Tuan Nguyen et al., "Improved Continuous Control Set Model Predictive Control for Three-Phase CVCF Inverters: Fuzzy Logic Approach," *IEEE Access*, vol. 9, pp. 75158-75168, 2021. [CrossRef] [Google Scholar] [Publisher Link]

[8] Min Chen et al., "Zero-Voltage-Switching Single-Phase Full-Bridge Inverter with Active Power Decoupling," *IEEE Transactions on Power Electronics*, vol. 36, no. 1, pp. 571-582, 2021. [CrossRef] [Google Scholar] [Publisher Link]

[9] Junjie Qin et al., "Thermal Balance Modulation of Switching Devices for Hybrid-Clamped Three-Level Full-Bridge LLC Resonant Converter," *IEEE Transactions on Power Electronics*, vol. 39, no. 5, pp. 5487-5497, 2024. [CrossRef] [Google Scholar] [Publisher Link]

[10] Zijiang Yang et al., "Resonant Current Estimation and Phase-Locked Loop Feedback Design for Piezoelectric Transformer-based Power Supplies," *IEEE Transactions on Power Electronics*, vol. 35, no. 10, pp. 10466-10476, 2020. [CrossRef] [Google Scholar] [Publisher Link]

[11] Shuo Chen et al., "Sensorless Control of PMSM Drives using Reduced Order Quasi Resonant-based ESO and Newton-Raphson Method-based PLL," *IEEE Transactions on Power Electronics*, vol. 38, no. 1, pp. 229-244, 2023. [CrossRef] [Google Scholar] [Publisher Link]

[12] Xiaoqiang Guo et al., "Leakage Current Reduction of Three-Phase Z-Source Three-Level Four-Leg Inverter for Transformerless PV System," *IEEE Transactions on Power Electronics*, vol. 34, no. 7, pp. 6299-6308, 2019. [CrossRef] [Google Scholar] [Publisher Link]

[13] Md Jahangir Hossain et al., "Multifunctional Three-Phase Four-Leg PV-SVSI with Dynamic Capacity Distribution Method," *IEEE Transactions on Industrial Informatics*, vol. 14, no. 6, pp. 2507-2520, 2018. [CrossRef] [Google Scholar] [Publisher Link]